

## Coherence resonance in an atmospheric global circulation model

Vicente Pérez-Muñuzuri\* and Roberto Deza†

Group of Nonlinear Physics, University of Santiago de Compostela, E-15782 Santiago de Compostela, Spain

Klaus Fraedrich, Torben Kunz, and Frank Lunkeit

Meteorologisches Institut, Universität Hamburg, Bundesstrasse 55, D-20146 Hamburg, Germany

(Received 30 July 2004; revised manuscript received 9 May 2005; published 27 June 2005)

Numerical evidence is presented of a coherence-resonant behavior, induced on an atmospheric global circulation model by a white (in time and space) additive Gaussian noise with amplitude  $A \ll 1$ . Intermediate  $A$  values enhance the spatiotemporal regularity of vortical patterns that contribute to the intra-annual variability of the atmospheric component of the climate. Only weak patterns (those appearing in the summer hemisphere) become ordered by noise.

DOI: 10.1103/PhysRevE.71.065602

PACS number(s): 92.60.Bh, 05.40.Ca, 92.70.Gt

The quest for understanding the sources of climate variability at the different timescales—a primary goal of climatology—has been spurred in the past quarter of a century by the global concern about anthropogenic climate change, since uncertainties in the former spoil the predictability with regard to the latter. The climate system is conceptually composed of subsystems with very different response timescales to perturbations, whose nonlinear (e.g., hydrodynamic) couplings connect the variabilities at different timescales, resulting in a broad variability spectrum. Although some of the present state-of-the-art coupled atmosphere-ocean (CAO) global circulation models (GCM)—albeit resorting to purely deterministic parametrizations—succeed to account for the high-frequency part of this spectrum (i.e., up to decades) [1], the need for a stochastic ingredient in the parametrization of subgrid processes has been recognized long ago [2]. The main reasons are the wide timescale separation between the component subsystems, the inherent uncertainties about the proper way to account for unresolved processes, and the experimental errors in the validatory measurements.

In fact, the well-known phenomenon of stochastic resonance (SR) [3,4]—a paradigm of the constructive effects of noise on nonlinear systems—can be regarded as a byproduct of this new trend in climatology, known as *stochastic parametrization* [5,6]. As it is known, the first attempted application of stochastic resonance, to the best of our knowledge, was to explain (within a very simple energy-balance model [7,8]) climatic variability at the glaciation timescale (a goal that seems to have been recently fulfilled in the more appropriate framework of a full-scale CAO—GCM [9,10]). A close relative of SR (also known as “internal” or “autonomous” stochastic resonance [11]) is the phenomenon of *coherence resonance* (CR) [12], wherein noise enhances the coherence of inherent modes of the system without the presence of periodic forcing as in SR: for an intermediate level of

noise, a peak appears in the spectral density at a given frequency. In this sense, it has been shown that millennial-scale climate oscillations can be excited stochastically, when the North Atlantic Ocean is fresh enough [10]. Other situations have been studied in the literature, both theoretically and experimentally, of which the most paradigmatic are *excitable systems* [12] and *noisy precursors* of a variety of bifurcations [11,13]. Regarding *extended* systems, noise-induced synchronization [14] has been observed in a 2D array of FitzHugh-Nagumo neurons, and the noisy precursor of the synchronized manifold’s Hopf bifurcation, in a ring of unidirectionally coupled Lorenz systems [15].

In this Rapid Communication, an instance of the CR phenomenon is described in the context of atmospheric dynamics and shown to contribute to intra-annual variability. The phenomenon appears far from the bifurcation to periodic solutions, when (following the stochastic parametrization philosophy) a simplified atmospheric GCM developed at Hamburg University—the so-called *Portable University Model of the Atmosphere* (PUMA) [16–18]—is forced with an additive Gaussian noise, white in time and space. The latter enhances the development and temporal regularity of circulation patterns arising in the atmosphere and ultimately related to the presence of a stable Rossby wave in mid-latitudes. Containing the dynamical core of atmospheric GCMs and very few (linear) parametrizations, PUMA yields realistic values and patterns for the zonally (i.e., longitudinally) averaged circulation and the transient waves [17–20].

The PUMA is a multilevel spectral model with triangular truncation, using the semi-implicit time integration as described in [16,21]. Longitude ( $\lambda$ ) and the sine of the latitude ( $\mu$ ) are the horizontal coordinates whereas in the vertical, terrain-following  $\sigma$  coordinates ( $\sigma = p/p_s$ ) are used. The vertical component ( $\zeta$ ) of the absolute vorticity (which includes Earth rotation), horizontal divergence ( $D$ ), temperature ( $T$ ), and the logarithm of the surface pressure ( $\ln p_s$ ) are its prognostic variables. The equations governing the former two stem from momentum balance; the one determining  $T$ , from the thermodynamic equation; and the one for  $\ln p_s$ , from mass conservation. Since the model resorts to the hydrostatic approximation, a fifth equation expresses such equilibrium in  $\sigma$  coordinates. The parametrizations are three: (a) Rayleigh

\*Corresponding author. Electronic address: vicente.perez@cesga.es

†Permanent address: Facultad de Ciencias Exactas, Universidad Nacional de Mar del Plata, Argentina.

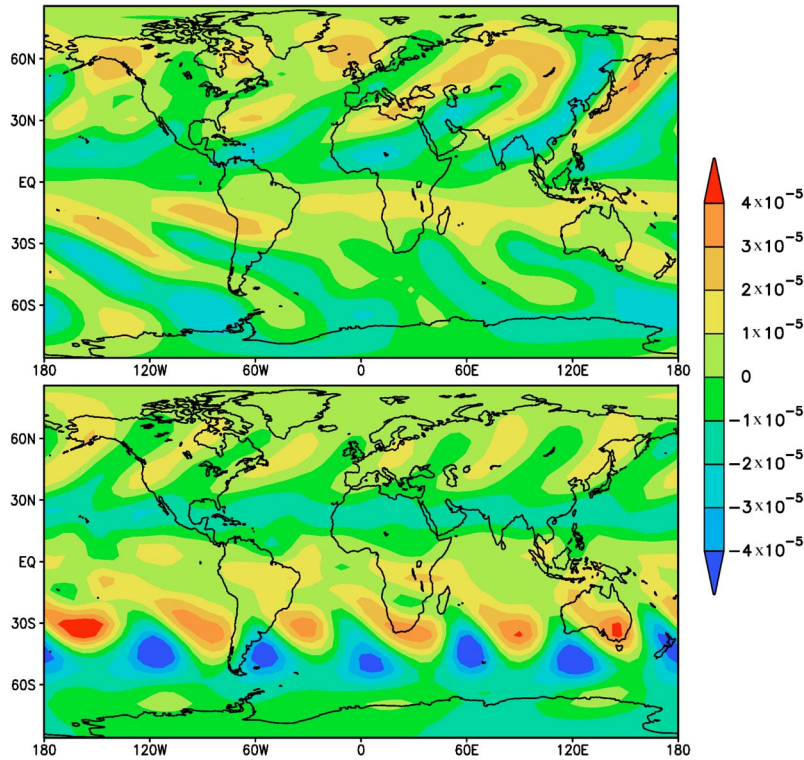


FIG. 1. (Color online) Vertical vorticity patterns observed at 300 hPa for two different values of the temperature difference between poles; above  $\Delta T_{NS}=0$  K (equinox conditions) and below  $\Delta T_{NS}=60$  K (permanent summer season in the northern hemisphere).

friction acting on  $\zeta$  and  $D$  (with a timescale  $\tau_f$ ) accounts for the large-scale dissipation processes; (b) a Newtonian cooling term (timescale  $\tau_N$  and reference temperature profile  $T_R$ ) parametrizes diabatic processes like radiation, sensible heat and cumulus convection; (c) hyperdiffusion terms in the equations for these three variables account for subgrid scale eddies.

For the simulations five vertical levels, a T21 horizontal resolution (approximately  $5.6^\circ \times 5.6^\circ$  on the corresponding Gaussian grid), and a time step of half an hour were chosen. The remaining parameters and scaling were the same as in [17,18]. Typical runs lasted 100 years, *neglecting the annual cycle* (i.e., under permanent season conditions). The first three years of each run were excluded, since during that qj-period the circulation was considered to establish from an initial field generated by adding to the  $(\ln p_s)$  field a white Gaussian noise of constant amplitude equal to  $10^{-3}$ . The effect of seasonal variability (intensity of the season) was introduced through  $\Delta T_{NS}$ , the pole-to-pole temperature difference at the Earth's surface:  $\Delta T_{NS}=0$  K corresponds to equinox conditions and  $\Delta T_{NS}>0$  K to the summer season in the northern hemisphere. The stochastic forcing was established by adding to the thermodynamic equation a Gaussian noise  $\eta(\mathbf{r}, t)$  with zero mean and correlation  $\langle \eta(\mathbf{r}, t) \eta(\mathbf{r}', t') \rangle = 2A \delta(\mathbf{r} - \mathbf{r}') \delta(t - t')$  [22].

Jet streams and synoptic (meteorological) scale disturbances are dominating features of the atmospheric circulation and its variability. Their interaction induces irregular low-frequency variability that affects the vortical patterns at a vertical level, as it is shown in Fig. 1 for 300 hPa and two different values of  $\Delta T_{NS}$ . Note that vortical patterns are reinforced in the southern [winter in Fig. 1] hemisphere as  $\Delta T_{NS}$  is increased.

Figure 2 depicts the time evolution of  $\zeta$ —and its corresponding power spectrum—at a given grid point ( $47^\circ$  N,  $0^\circ$  E), in the case of Fig. 1(b) and for three different noise amplitudes. For the intermediate value  $A=4 \times 10^{-5}$ , the series appears more regular, which is confirmed by the power spectrum (narrowest and highest peak). For very low values of noise, the peak around the mean frequency is wider and lower. For large noise amplitudes the power spectrum becomes broadband, and intermittent regions of noisy periodic oscillations and noise-dominated regions are observed. These

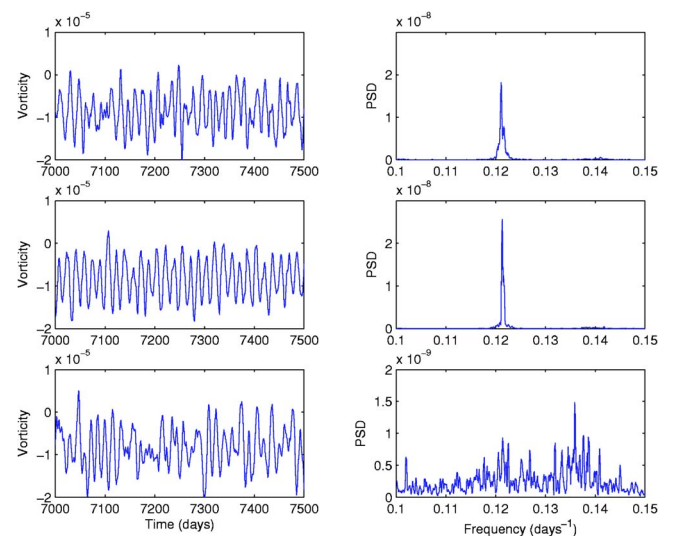


FIG. 2. (Color online) Vorticity time series (left) and their respective power spectra (right) in the summer hemisphere at ( $47^\circ$  N,  $0^\circ$  E), for  $\Delta T_{NS}=60$  K. From top to bottom:  $A=10^{-7}$ ,  $A=4 \times 10^{-5}$ , and  $A=4 \times 10^{-3}$ .

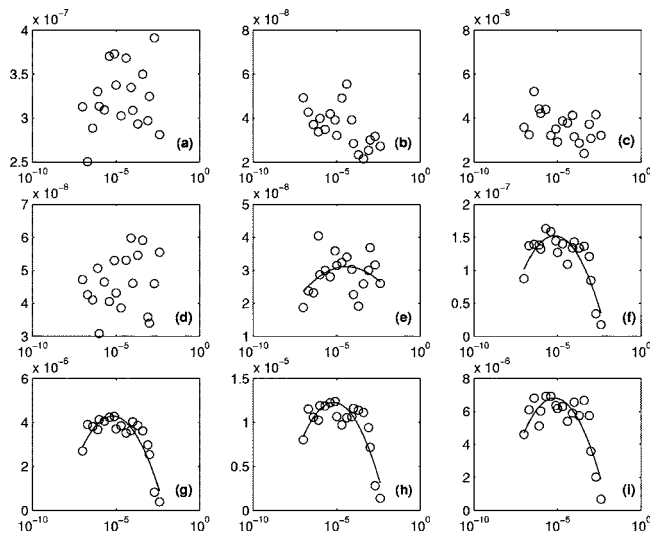


FIG. 3. Coherence factor  $\beta$  as a function of  $A$  for  $\Delta T_{NS}=60K$ , at  $0^\circ$  E and nine sampled latitudes from panels (a) to (i):  $47^\circ$  S,  $30^\circ$  S,  $14^\circ$  S,  $3^\circ$  N,  $14^\circ$  N,  $30^\circ$  N,  $47^\circ$  N,  $64^\circ$  N, and  $75^\circ$  N, respectively. Fitting curves are shown only to guide the eye at those latitudes where a functional relation is statistically compatible with data. Maximum errors for panels (a) to (i) are 10%, 17%, 15%, 17%, 17%, 14%, 13%, 15%, and 16%, respectively [23].

observations point to a resonant behavior since the temporal evolution of the pattern becomes more regular as  $A$  is increased, but this regularity becomes deteriorated past some optimal value of  $A$ .

To characterize quantitatively the observed ordering, we compute as functions of the noise amplitude  $A$  two measures traditionally used to study coherence resonance: the *coherence factor* [11]

$$\beta = H/W, \quad (1)$$

where  $H$  is the height and  $W$  the relative width of the dominant peak in the power spectrum (the higher and/or narrower the peak, the larger the temporal regularity of the vortical pattern), and the *characteristic correlation time* [12]

$$\tau_c = \int_0^\infty C^2(t) dt. \quad (2)$$

Both are calculated from the correlation function

$$C(\tau) = \frac{\langle \tilde{\zeta}(t) \tilde{\zeta}(t+\tau) \rangle}{\langle \tilde{\zeta}^2 \rangle}, \quad \tilde{\zeta} = \zeta - \langle \zeta \rangle, \quad (3)$$

$\zeta(t)$  being calculated at different latitudes, and at constant longitude ( $0^\circ$  E) [23].

Figures 3 and 4 show that both measures exhibit a non-trivial behavior as a function of  $A$ . Moreover, this behavior is markedly pronounced at midlatitudes in the summer hemisphere [e.g., panels (g,h)]. Both  $\beta$  and  $\tau_c$  exhibit a maximum at intermediate  $A$  values, which means that the vorticity time series becomes more regular, as expected for coherence resonance [12]. The effect of noise on the global circulation is more pronounced in the summer hemisphere, where the am-

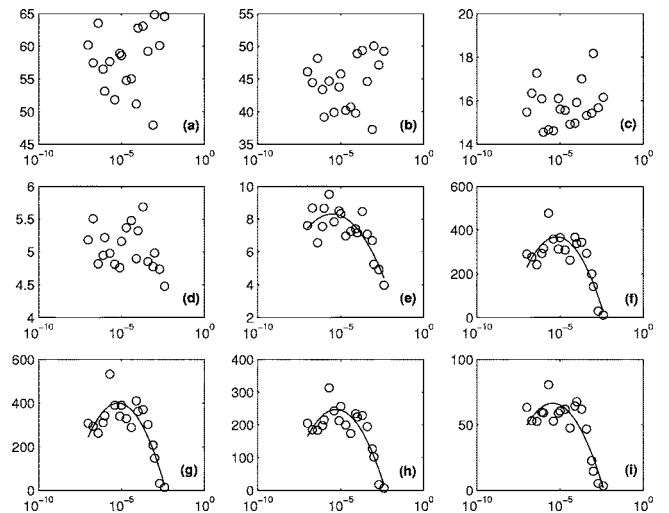


FIG. 4. Time correlation  $\tau_c$  as a function of  $A$  for the same latitudes and parameters as in Fig. 3. Maximum errors for panels (a) to (i) are 8%, 9%, 6%, 6%, 10%, 14%, 14%, 14%, and 15%, respectively [23].

plitude of the deterministic signal is weaker (i.e., the absolute values of  $\zeta$  are smaller than in the winter hemisphere). In the case of  $\beta$ , both an increase in  $H$  and a decrease in  $W$  contribute to maximize the coherence for some intermediate value of noise. For high noise intensities (in the summer hemisphere)  $\beta$  goes to zero since the spectrum becomes broadband (Fig. 2, bottom), leading to smaller values of  $H$  than of  $W$ . For low noise intensities, neither  $\beta$  nor  $\tau_c$  tend to zero (Poissonian limit) since the noiseless model exhibits a quasiperiodic behavior. Although the vorticity time series shows a periodic behavior for low  $A$ , the ratio  $H/W$  is smaller than for intermediate noise intensities (see, for example, the spectral densities in Fig. 2).

The effect of white noise is more relevant for midlatitudes in the summer hemisphere, where  $\beta$  and  $\tau_c$  attain their maximum values. At these latitudes the deterministic vortical pattern is neither ordered nor strong enough to clearly stand out above the background, although a pattern of waves with zonal wave number  $\sim 6$  circling the globe can be easily appreciated from Fig. 1. Zonal wave number 6 (mode-6) is the dominant one in the sense that it is most responsible for the fluctuations at a gridpoint induced by the corresponding traveling mode-6 pattern. Figure 5 shows the contribution of each spectral mode of the vorticity field to  $\beta$  and  $\tau_c$  at the midlatitude analyzed and for three different values of noise intensity. Note that mode-6 contributes most strongly to the enhanced regularity measured by  $\beta$  and  $\tau_c$  (see also Figs. 3 and 4) compared to the remaining modes and attains a maximum value for an intermediate level of noise. And thus it proves to be the mode responsible for the CR phenomenon. The midlatitude systems appear more regularly aligned along a latitude circle and show reduced north-south fluctuations of the positions of their centers. Besides, mode-7 is excited for large noise intensities, as the pattern becomes more disordered.

Hence, adding noise to a pre-existing (nearly ordered) pattern reinforces the resonance. On the other hand, for the

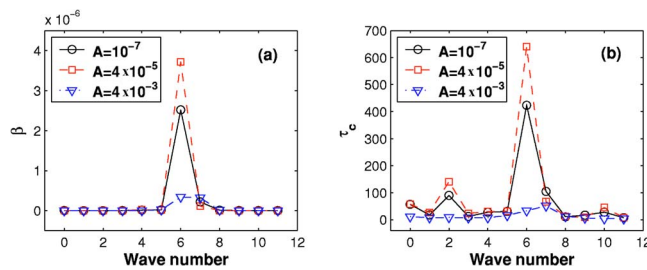


FIG. 5. (Color online) Coherence factor  $\beta$  (a) and time correlation  $\tau_c$  (b) as a function of wave number for three different values of  $A$ . Note the resonant peaks observed for wave numbers 2 and 10 in panel (b). In both cases, ( $47^\circ$  N,  $0^\circ$  E) and  $\Delta T_{NS}=60$  K.

winter hemisphere—independently of the latitude—vortical patterns are so well defined that noise cannot affect their behavior. The meaning of  $\beta$  and  $\tau_c$  being different from zero in the winter hemisphere is that some oscillatory behavior exists in the model dynamics, but no ordering (i.e., a bell-shaped functional dependence on  $A$  as expected for coherence resonance and observed in the summer hemisphere) occurs as noise increases.

The difference in behavior observed in each hemisphere for  $\Delta T_{NS} > 0$  can be interpreted by resorting to the simple stochastic model described in [15]. Since the zonal vortical patterns are long wavelength features, the zonal behavior of the vorticity at constant latitude in both hemispheres is roughly equivalent to their problem, namely the (noise-assisted) instability of the invariant subspace in a bounded system. The mean first-passage frequency thus obtained is an increasing function of  $A$ , and equals the deterministic wave frequency (that hardly changes with noise) at some optimal noise level  $A^*$ . In our case, the deterministic mean frequency in the summer hemisphere is four times smaller than in the winter one. Thus, in order to obtain a resonance in the winter

hemisphere,  $A_w^*$  should be larger than  $A_s^*$  in the summer one, in fact, so large that it would mask the weak deterministic signal existing in the summer hemisphere.

Our results suggest that noise has the ability to enhance predictability of vortical patterns in such high-dimensional systems as a atmospheric GCM by generating higher regularity. In nature, there are additional causes for the variability of vortical structures (they are influenced by orography, moist processes, etc., which are not solved by PUMA). Nevertheless, wind anomalies which originate in the tropics and propagate slowly poleward do occur in the atmosphere and tend to be much more coherent in the summer hemisphere than in the winter one [24]. A plausible explanation for this different behavior could be the presence of noise, which being ubiquitous in nature and in atmospheric models (e.g., in turbulence parameterizations), makes the weaker summer-hemisphere structures appear in a more regular fashion. These results highlight the potential of introducing noise into numerical weather prediction (NWP) models where noise-amplitude becomes a crucial parameter. A consequence for NWP strategy is to perform forecasts with ensemble sets forced by different noise levels. In the experiments above, noise is added at each time step which, in a first approximation, is independent in space and in time. However, uncorrelated noise may be a too idealistic assumption in general. In particular, the introduction of noise correlated in space and time has significant influence on, for example, ensemble weather forecasting [18].

This work was supported by Xunta de Galicia under Research Grant No. PGIDT01MAM20802PR and by the European Science Foundation (ESF) Grant *STOCHDY*. Linkage Germany – Spain [HA2003-0112 (MCyT); PKZ:D/03/39285 (DAAD)]. EC-NEST (Extreme Events-Causes and Consequences), and SFB-512 (Tiefdruckgebiets und Klimasystem des nordatlantiks).

- 
- [1] K. Fraedrich and R. Blender, *Phys. Rev. Lett.* **90**, 108501 (2003).
- [2] K. Hasselmann, *Tellus* **28**, 473 (1976).
- [3] C. Nicolis and G. Nicolis, *Tellus* **33**, 225 (1981).
- [4] R. Benzi, A. Sutera, and A. Vulpiani, *J. Phys. A* **14**, L453 (1981).
- [5] J. W. B. Lin and J. D. Neelin, *J. Atmos. Sci.* **59**, 959 (2002).
- [6] B. Khouider, A. J. Majda, and M. A. Katsoulakis, *Proc. Natl. Acad. Sci. U.S.A.* **100**, 11941 (2003).
- [7] C. Nicolis, *Tellus* **34**, 1 (1982).
- [8] R. Benzi, A. Sutera, and A. Vulpiani, *Tellus* **34**, 10 (1982).
- [9] A. Ganopolski and S. Rahmstorf, *Phys. Rev. Lett.* **88**, 038501 (2002).
- [10] A. Timmermann, H. Gildor, M. Schultz, and E. Tziperman, *J. Clim.* **16**, 2569 (2003).
- [11] H. Gang, T. Ditzinger, C. Z. Ning, and H. Haken, *Phys. Rev. Lett.* **71**, 807 (1993).
- [12] A. S. Pikovsky and J. Kurths, *Phys. Rev. Lett.* **78**, 775 (1997).
- [13] V. S. Anishchenko, V. Astakhov, A. B. Neiman, T. Vadivasova, and L. Schimansky-Geier, *Nonlinear Dynamics of Chaotic and Stochastic Systems* (Springer-Verlag, Berlin, 2002).
- [14] Y. Shinohara, T. Kanamaru, H. Suzuki, T. Horita, and K. Aihara, *Phys. Rev. E* **65**, 051906 (2002).
- [15] M. Zhan, G. W. Wei, C.-H. Lai, Y.-C. Lai, and Z. Liu, *Phys. Rev. E* **66**, 036201 (2002).
- [16] K. Fraedrich, E. Kirk, and F. Lunkeit, *DKRZ Tech. Rep. No. 16*, 1998, <http://puma.dkrz.de/puma>.
- [17] F. Lunkeit, *Chaos* **11**, 47 (2001).
- [18] V. Pérez-Muñuzuri, M. N. Lorenzo, P. Montero, K. Fraedrich, E. Kirk, and F. Lunkeit, *Nonlinear Processes Geophys.* **10**, 1 (2003).
- [19] I. N. James and P. M. James, *Nature (London)* **342**, 53 (1989).
- [20] P. M. James, K. Fraedrich, and I. N. James, *Q. J. R. Meteorol. Soc.* **120**, 1045 (1994).
- [21] B. J. Hoskins and A. J. Simmons, *Q. J. R. Meteorol. Soc.* **101**, 637 (1975).
- [22] Noise amplitude units are  $K/day$  with scaling as in [17,18]. The set of  $A$  values used through this paper is of the same order of magnitude as the subscale heating rates in convectively active atmospheric columns ( $\sim 1 K/day$ ).
- [23] Ensemble averages of Eqs. (1) and (2) are performed over 20 noise realizations. Errors are calculated as standard deviations of the mean value, normalized by the maximum value.
- [24] T. Riehl, C. Yeh, and N. E. LaSeur, *J. Meteorol.* **7**, 181 (1950).